RIDI
Revista de Investigación
Desarrollo e Innovación

Proposal of a computational method for asbestos detection in hyperspectral images based on the identification of prominent peaks in the spectral signature

Propuesta de un método computacional para la detección de asbesto en imágenes hiperespectrales a partir de la identificación de los máximos prominentes de la firma espectral

Research article

Recibido: diciembre 11 de 2024
Aceptado: febrero 20 de 2025
Publicado: marzo 31 de 2025

Cómo citar este artículo: Chanchí-Golondrino, G. E., Ospina-Alarcón, M. A., & Saba, M. (2025). Proposal of a computational method for asbestos detection in hyperspectral images based on the identification of prominent peaks in the spectral signature. *Revista de Investigación, Desarrollo e Innovación, 15* (1), 119-138.

doi: https://doi.org/10.19053/uptc.20278306.v15.n1.2025.19183

Gabriel Elías Chanchí-Golondrino*
Universidad de Cartagena, Cartagena de Indias, Colombia.
E-mail: gchanchig@unicartagena.edu.co
Orcid: https://orcid.org/0000-0002-0257-1988

Manuel Alejandro Ospina-Alarcón
Universidad de Cartagena, Cartagena de Indias, Colombia.
E-mail: mospinaa@unicartagena.edu.co
Orcid: https://orcid.org/0000-0003-4510-0753

Manuel Saba
Universidad de Cartagena, Cartagena de Indias, Colombia.
E-mail: msaba@unicartagena.edu.co
Orcid: https://orcid.org/0000-0003-1345-9657

Abstract

This study proposes a computational method for asbestos detection in hyperspectral images. The methodology consists of five phases: selection of sample pixels and identification of the characteristic pixel, determination of prominent peaks in the spectral curve, method implementation with reference threshold definition, application to test images, and comparative evaluation of eff ctiveness and efficiency. The method identifies asbestos pixels by calculating the Euclidean distance between the prominent peaks of spectral curves. Results show no overlap between maximum distances of asbestos pixels and minimum distances of non-asbestos pixels, detecting 11.87% of asbestos pixels in the test image. Although the correlation method is 1.02% faster, the diff rence is negligible. This method can be extrapolated to other materials with similar spectral features, contributing to urban diagnostics of hazardous materials like asbestos.

Keywords: asbestos, hyperspectral imaging, maximum detection, remote sensing.

Resumen

Este estudio propone un método computacional para detectar asbesto en imágenes hiperespectrales. La metodología incluye cinco fases: selección de píxeles de muestra y obtención del píxel característico, determinación de los picos prominentes de la curva espectral, implementación del método con definición de umbrales de referencia, aplicación del método a imágenes de prueba, y evaluación comparativa de efectividad y eficiencia. El método identifica píxeles de asbesto calculando la distancia euclidiana entre los picos prominentes de las curvas espectrales. Los resultados muestran que no hay traslape entre las distancias máximas de píxeles de asbesto y las mínimas de no asbesto, logrando detectar el 11.87% de píxeles de asbesto en la imagen de prueba. Aunque el método de correlación es 1.02% más rápido, la diferencia es mínima. Este método puede ser aplicado a otros materiales y contribuye al diagnóstico urbano de materiales peligrosos como el asbesto.

Palabras clave: asbesto, imágenes hiperespectrales, detección de máximos, sensado remoto.

1. Introduction

Hyperspectral remote sensing involves the use of sensors that capture hundreds of narrow, contiguous spectral bands spanning from the ultraviolet range, through the visible and near-infrared, to the shortwave infrared. This provides high spectral resolution, enabling detailed characterization of materials and their physical or chemical states (Adão et al., 2017; Eismann, 2012; González-Núñez & de la Fuente, 2017; Sahoo, 2020). Hyperspectral sensors can be mounted on satellites, airplanes, drones, or even used in laboratories and fi ld settings, allowing the measurement of surface reflectance and material properties across different spectral bands (Gu et al., 2021). One of the main advantages of hyperspectral remote sensing is its ability to detect and classify materials non-invasively, leveraging the capture, processing, and analysis of Hyperspectral Images (HSI). This enables the use of material reflectance properties for identification without the need for direct intervention or physical contact (Pérez-Roncal et al., 2019). In this context, HSI is acquired using imaging spectrometers that collect data across multiple, closely spaced spectral bands, providing both spatial and spectral information about observed objects (Zhang & Zhong, 2010). HSI is typically represented as hyperspectral datacubes, defined as three-dimensional matrices capturing spatial images in two dimensions and spectral data in the third. Each pixel in the spatial dimensions (x, y) contains a complete wavelength spectrum, offering detailed information about the physical and chemical properties of the observed area (Bodkin et al., 2009; Gao & Smith, 2015; Lim & Murukeshan, 2017; Park, 2016).

HSI processing and analysis have been applied across various fields, including environmental science, agriculture, geology, and military security. In the environmental field, HSI technology has been utilized in remote sensing applications for water resource management, enabling the assessment of water quality and the detection of pollutants (Khan et al., 2018). Similarly, HSI has been used to create spatial distribution maps of physical and ecological terrain features, such as chlorophyll content in vegetation, for assessing plant health and identifying contaminated areas (Moroni et al., 2013). Moreover, HSI has been employed to produce high-precision image mosaics of urban areas, rivers, and forests, facilitating the evaluation of spectral fidelity, terrain geometry, changes in land cover, vegetation health, and water quality (Yi et al., 2021). In agriculture, HSI has been widely adopted for monitoring crop health, allowing early detection of diseases and stress factors, thus enabling timely interventions (Ang & Seng, 2021; Lu et al., 2020; Wang et al., 2021). Additionally, HSI has been used for the rapid, non-destructive identification of microplastics in agricultural soils, employing data processing techniques such as Principal Component Analysis (PCA) and classification models like Convolutional Neural Networks (CNN) (Ai et al., 2022). HSI has also proven effective in estimating the presence of heavy metals such as Chrome (Cr), Copper (Cu), and Lead (Pb) in agricultural soils, utilizing Spectral Analysis Models (SAM) and Machine Learning Techniques (MLT) (Tan et al., 2020). In geology, HSI has been predominantly applied in mineral mapping, enabling the precise identifi ation of various mineral types within a specific region (Gao et al., 2017; Peyghambari & Zhang, 2021). In the military context, HSI plays a critical role in detecting vessels, vehicles, and camouflage on the battlefi ld. It accurately characterizes surface materials and facilitates the detection of concealed or low-signature targets, providing a significant strategic advantage by enabling sub-pixel recognition and identifying terrain disturbances (Mendes et al., 2010; Paoletti et al., 2019).

On the other hand, considering the focus of this research and the importance of detecting materials like asbestos for public health, HSI has been used to identify asbestos-containing materials in construction and demolition waste. This has been achieved by employing Shortwave Infrared (SWIR) images combined with multivariate classification methods such as Hierarchical Partial Least Squares Discriminant Analysis (HI-PLSDA) and Support Vector Machines (SVM) (Bonifazi et al., 2024). Similarly, HSI in the SWIR range (1000-2500 nm) has been applied to detect and classify various asbestos minerals, including amosite, crocidolite, and chrysotile, in cement matrices. This has been done using techniques based on the identification of specific spectral signatures, such as hydroxyl combination bands (Mg-OH and Fe-OH) (Bonifazi et al., 2015, 2018, 2019). In urban environments, tools like Environment for Visualizing Images (ENVI) have been used for processing and analyzing HSI to identify fiber cement or asbestos in Cartagena de Indias, Colombia, revealing that up to 47% of certain neighborhoods were covered with this material (Valdelamar-Martínez et al., 2024). Similarly, it has been demonstrated that HSI combined with machine learning techniques can effectively identify asbestos-containing fiber cement roofs, achieving remarkable accuracy (Abbasi et al., 2022; Frassy et al., 2014; Kaplan et al., 2023).

Considering that HSI has high dimensionality, as it corresponds to datacubes with a depth equivalent to hundreds of reflectance bands, this high dimensionality increases computational costs and storage requirements, making efficient processing challenging (Eckhard et al., 2015; González et al., 2010; Kapre et al., 2023). Similarly, the high dimensionality of HSI not only leads to an increase in data volume but also introduces issues such as data redundancy, the Hughes phenomenon, and complexity in processing and analyzing information. The Hughes phenomenon refers to the degradation of classifi ation performance as dimensionality increases, which can result in overfitting of machine learning models (Ding et al., 2016; Islam et al., 2024). Moreover, it is important to note that HSI processing faces computational challenges related to algorithmic complexity. While the effectiveness of machine learning and deep learning algorithms has been demonstrated, these approaches require significant computational resources and are susceptible to overfitting due to the high dimensionality of the data (Islam et al., 2024; Zhang et al., 2020). Therefore, it is essential to develop computational methods that focus not only on the effectiveness of material detection using HSI but also on computational efficiency.

Based on the above, this article proposes a novel mathematical method for identifying asbestos in hyperspectral images. The method is based on detecting image pixels whose most prominent peaks have the smallest Euclidean distance to the most prominent peaks of the asbestos spectral signature. This approach leverages the fact that spectral signature curves of materials exhibit unique characteristic peaks across different reflectance bands, which act as distinctive identifiers. By focusing on the most significant spectral features, this method aims to improve the accuracy and reliability of asbestos detection. To evaluate the effectiveness and efficiency of the proposed method, a reference hyperspectral image of the Manga neighborhood in Cartagena de Indias was used. The method was assessed using asbestos and non-asbestos pixels to identify detection thresholds and subsequently validate the method on the full image. This method was implemented using open-source libraries (spectral, scipy, numpy, pandas, and matplotlib) and is designed to serve as a reference for both academic and industrial applications. It also has the potential to be extrapolated for detecting other materials and integrated into hyperspectral image analysis tools. Furthermore, this method represents a significant contribution to public health by enabling precise urban diagnostics of asbestos presence. This is particularly relevant given the severe health implications of asbestos, including its association with respiratory diseases such as asbestosis, lung cancer, and mesothelioma.

The remainder of the article is organized as follows: Section 2 outlines the methodological phases that guided the development of this research. Section 3 describes the results obtained, which include the determination of the asbestos spectral signature from sample pixels and their most prominent peaks, the implementation and evaluation of the proposed method using asbestos sample pixels and pixels from other materials to establish detection thresholds, the assessment of the effectiveness in detecting asbestos pixels within the reference hyperspectral image by comparing the results to the correlation method, and finally, the evaluation of the computational efficiency of the proposed method relative to the correlation method. Lastly, Section 4 presents the conclusions and future work derived from this research.

2. Methodology

For the development of this research, five methodological phases were defined (see Figure 1): P1. Selection of sample pixels and determination of the characteristic pixel, P2. Identification of the most prominent peaks of the characteristic pixel, P3. Implementation and determination of the method's reference thresholds, P4. Application of the method to the reference image, and P5. Comparative evaluation of the proposed method.

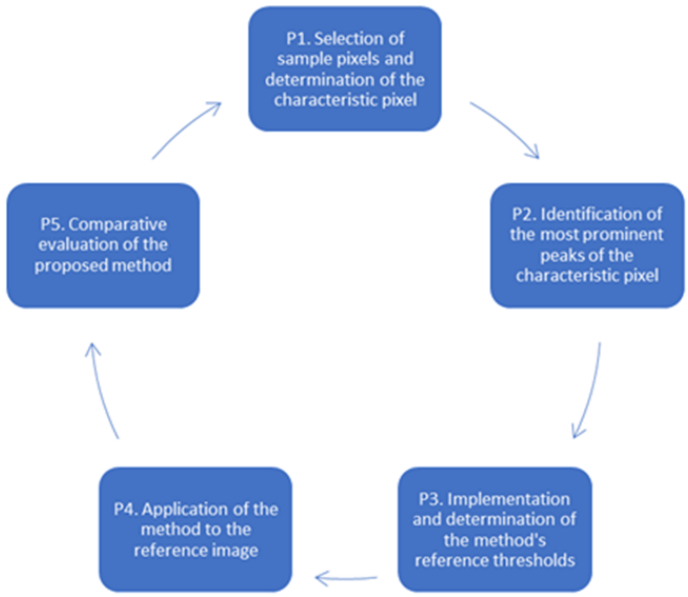

Figure 1. Methodology considered.

In the first phase of the methodology, an initial set of 75 asbestos pixels and 75 non-asbestos pixels (including vegetation, freshwater, roads, metal roofs, among others) were selected from a reference hyperspectral image of the Manga neighborhood in the city of Cartagena. This image has a width of 850 pixels, a height of 725 pixels, and comprises a total of 380 spectral or reflectance bands. These sample pixels served as the basis for obtaining the average asbestos pixel or reference spectral signature of asbestos, as well as for determining the reference threshold from which the method can detect asbestos pixels. Thus, in Figure 2, the selected asbestos pixels are displayed in blue on the reference hyperspectral image, while the selected pixels of other materials are shown in red. It is worth mentioning that Figure 2 also presents the image scale and the cardinal orientation.

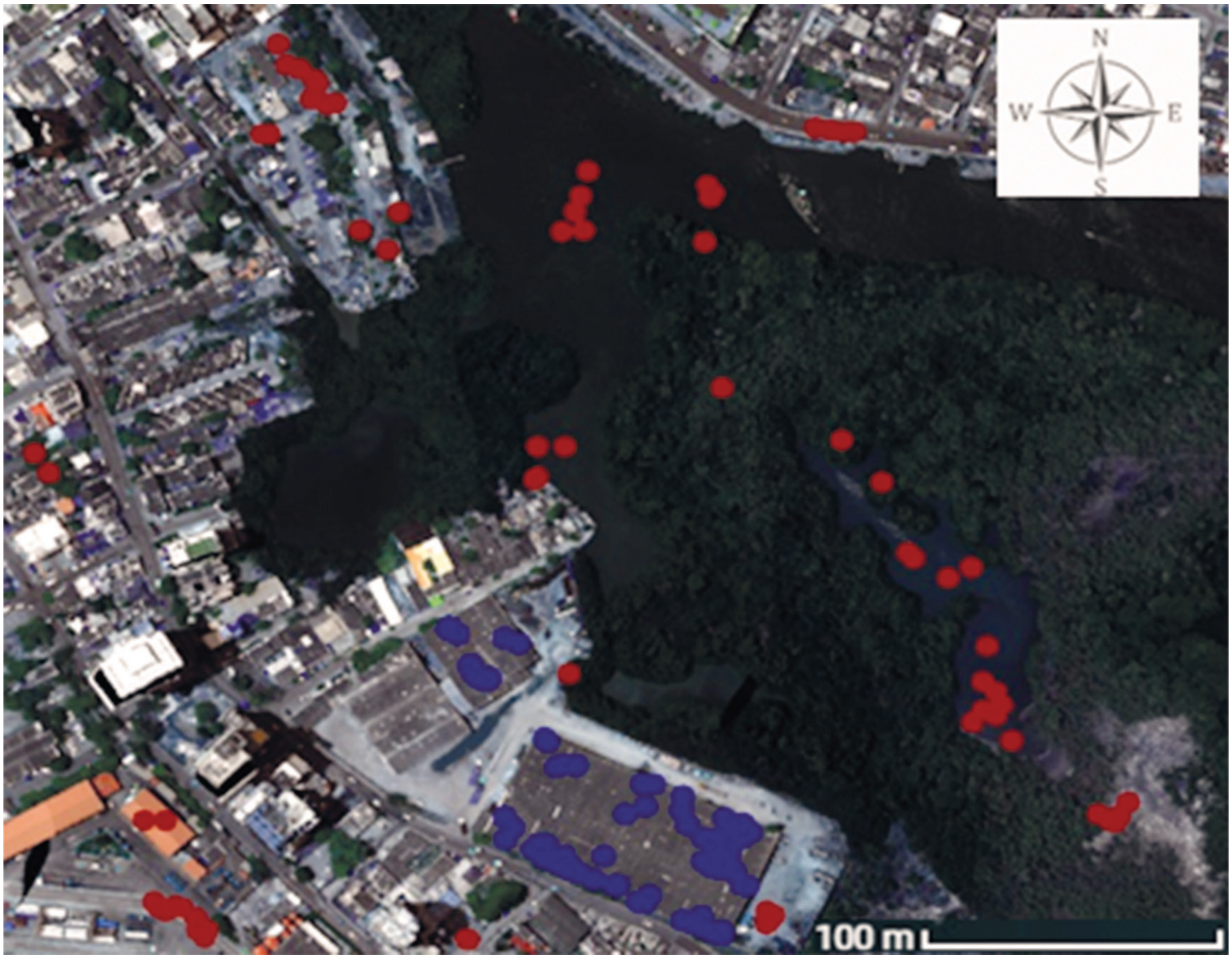

Figure 2. Reference hyperspectral image.

Starting from the 75 selected asbestos pixels, the characteristic asbestos pixel was obtained. This pixel encompasses the normalized reflectance average of the asbestos pixels across its 380 bands (see Figure 3). It is worth mentioning that this pixel proves highly useful, as it was subsequently employed to operate and correlate with various pixel types to determine the similarity between the characteristic asbestos pixel and the sample pixels from the image.

In phase 2 of the methodology, the determination of prominent peaks at the level of the characteristic or average pixel was carried out, utilizing the advantages provided by the find_peaks() function from Python's SciPy library. In this process, the find_peaks() method was configured to identify peaks with a prominence greater than 0.025 and a height exceeding 0.196 in the normalized asbestos spectral signature. This was achieved by characterizing the various peaks identified in the curve, prioritizing the most relevant ones. The prominence of a peak in a curve is a measure describing the relative height of a peak compared to its surroundings and can be defined as the difference between the peak height and the lowest level of the nearest valley connecting that peak to another higher peak or the curve's boundaries. It is worth noting that the fi d_peaks() method leverages the advantages of the first and second derivatives of the curve, detecting a maximum when the first derivative is zero and the second derivative is negative. The prominence of the peaks is calculated as the difference between the peak height and the highest level of the adjacent valleys (left and right). Specifically, the prominence is determined by subtracting the highest value of f(x) corresponding to the minimum points on either side from the peak value, thus evaluating the relative significance of the peak in its immediate context. Accordingly, Equations (1) and (2) represent the mathematical operations performed by the find_peaks() method of the SciPy library to detect the most prominent peaks in the specific case of the asbestos spectral signature. It is important to highlight that, since the detected peaks are located before the 300th reflectance band, only the first 300 bands were considered in the subsequent phases.

$$f'(x_i) = 0, f''(x_i) < 0 \ \ y \ f(x_i) - \max\left(f(x_{left\,Valley}), f(x_{right\,valley})\right) \geq 0.0125 \quad (1)$$

$$(x_i) \geq 0.196 \quad (2)$$

Once the most prominent peaks and the reflectance bands where these peaks are located were detected, phase 3 focused on determining the Euclidean distance between the array formed by the spectral signature peak bands and the array of reflectance bands corresponding to the peaks obtained for each of the 75 asbestos and non-asbestos pixels. In this way, distance thresholds were established, enabling the method to determine whether a given pixel is asbestos or not, ensuring beforehand that there is no overlap between the maximum distance calculated for asbestos pixels and the minimum distance obtained for non-asbestos pixels.

Using the reference thresholds identifi d in phase 3 as a starting point, phase 4 of the methodology involved applying the proposed method to each pixel of the reference hyperspectral image. This process included counting the identified pixels and calculating the percentage of pixels classified as asbestos relative to the total number of pixels. As previously mentioned, the Euclidean distance between the reflectance bands of the reference pixel peaks and the peaks of the image pixels was calculated using only the fi st 300 reflectance bands, excluding the remaining 80 bands.

Finally, in phase 5 of the methodology, the effectiveness and efficiency of the proposed method in detecting asbestos pixels were analyzed. Regarding effectiveness, the percentage of pixels detected by the proposed method was compared to the percentage detected by the correlation method. Similarly, in terms of efficiency, a region of the hyperspectral image measuring 50x50 pixels was selected, and 20, 40, 60, 80, and 100 executions of the proposed method and the correlation method were performed. This allowed for a comparison of the average processing time of each method and the determination of the proposed method's efficiency in relative terms.

3. Results and discussion

Firstly, regarding the results, the average asbestos pixel was obtained from the 75 selected asbestos sample pixels, utilizing the advantages provided by the NumPy library. The characteristic pixel was derived by calculating the band-by-band average of the 75 reference pixels, considering only the first 300 reflectance bands. Thus, Figure 3 presents both the spectral signature of the 75 asbestos pixels and the characteristic spectral signature or average asbestos pixel, in both cases limited to the first 300 bands.

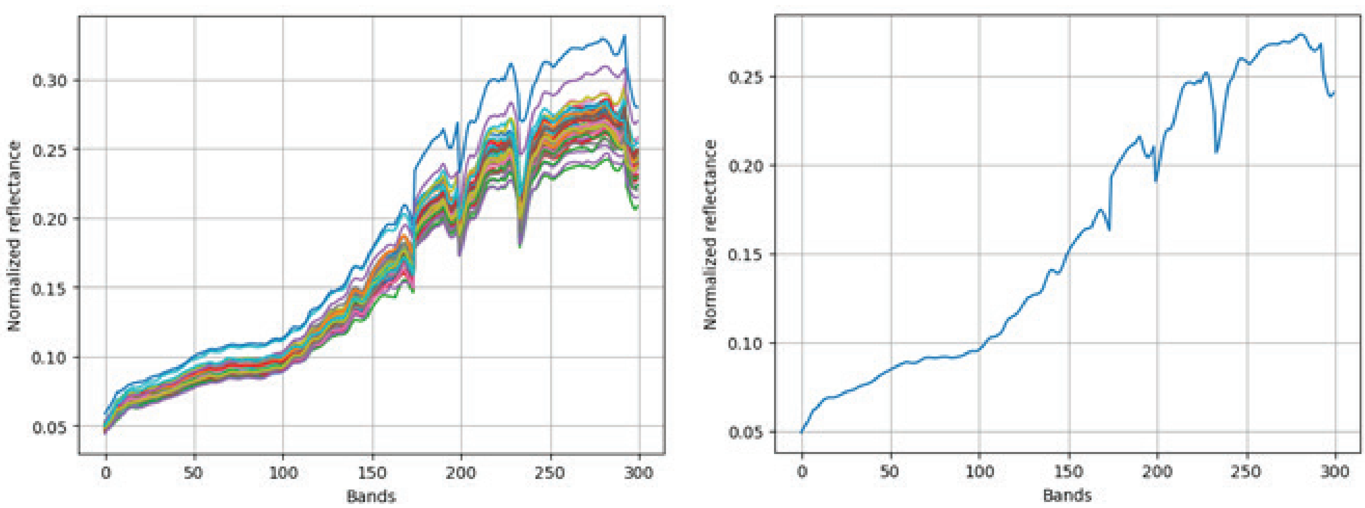

Figure 3. Asbestos sample pixels and obtained average pixel.

Once the average pixel was obtained, the relevant peaks of the asbestos spectral signature were identifi d, considering only those peaks with a prominence greater than 0.025 and a height exceeding 0.196 in the normalized asbestos spectral signature. Thus, the three relevant peaks presented in Figure 4 were identifi d, located at reflectance bands 190, 227, and 281, with respective prominences of 0.025, 0.045, and 0.035.

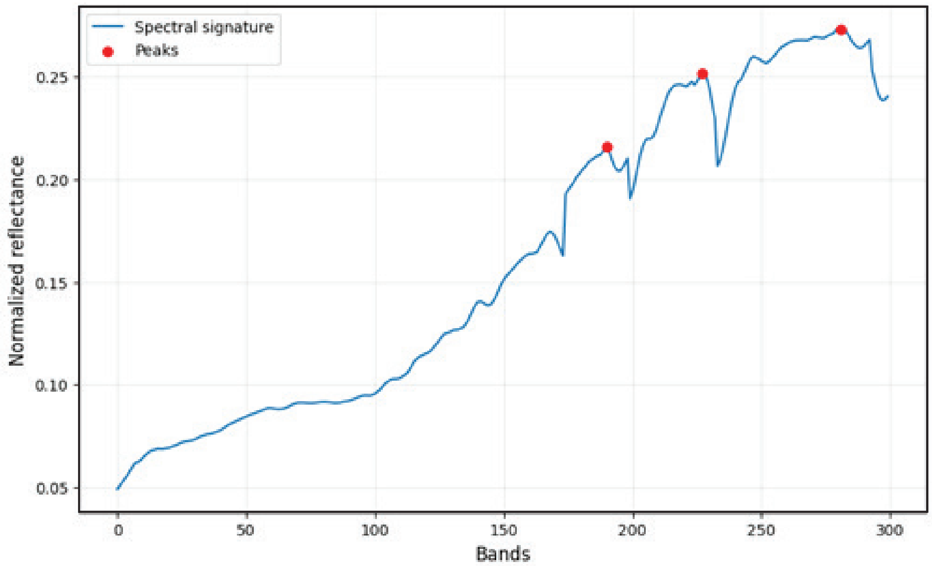

Figure 4. Peaks with highest prominence detected in the asbestos spectral signature.

Once the relevant peaks in the asbestos spectral signature were identified, the Euclidean distance was calculated between the bands of these peaks and the bands of the peaks determined in the sample pixels, using the Python script shown in Figure 5. This script illustrates the iteration over the 75 asbestos pixels, the calculation of peaks in each iteration, and the determination of the Euclidean distance for each pixel. This process leveraged the advantages provided by the find_peaks() function from the SciPy library for peak detection and the linalg. norm() function from the NumPy library for calculating the Euclidean distance. It is worth noting that a similar script was applied for the non-asbestos pixels, in which the iteration was performed over the list of 75 non-asbestos pixels.

```
import scipy.spatial.distance as ssd

def eu_norm(vector1, vector2):
  # Calculate the Euclidean distance between the two arrays
  dist_eu = np.linalg.norm(vector1 - vector2)
  return dist_eu

l_dist=[]
k=1
for i in range(0,len(l_pix_asb)):
  pix=l_pix_asb[i]
  # We use the find_peaks function to identify the indexes of the peaks
  # Finding relevant peaks
  peaks, properties = find_peaks(pix[:300], prominence=0.02, height=0.196)
  pic_pix=peaks[:3]

  dist=eu_norm(pic_pix, all_peaks)
  l_dist.append(dist)
  k+=1
arr_porc_asb=np.asarray(l_dist)
print(f"Avg: {round(arr_porc_asb.mean(),3)}")
print(f"Min: {round(arr_porc_asb.min(),3)}")
print(f"Max: {round(arr_porc_asb.max(),3)}")
```

```
Avg: 3.287
Min: 0.0
Max: 13.638
```

Figure 5. Script for the evaluation of the method with asbestos pixels.

Thus, after applying the proposed method to the asbestos and non-asbestos pixels, the results presented in Figure 6 were obtained, showing the minimum, maximum, and average Euclidean distances calculated by the method for both asbestos and non-asbestos pixels.

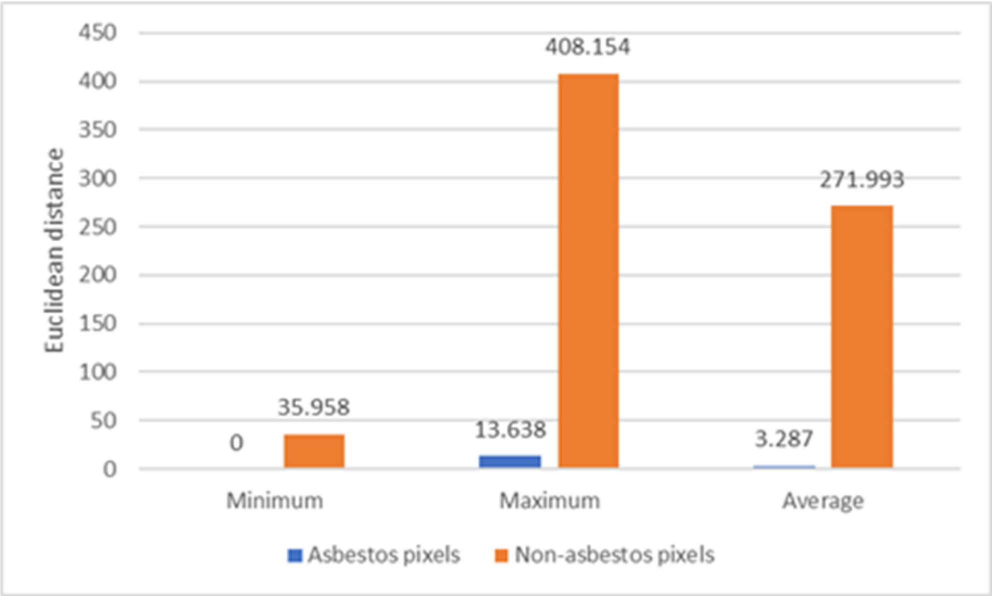

Figure 6. Evaluation of the proposed method with asbestos and non-asbestos pixels.

According to the results shown in Figure 6, it can be observed that the maximum Euclidean distance obtained between the bands of the relevant peaks of the characteristic pixel and the bands of the peaks of the asbestos pixels was 13.638, while the minimum Euclidean distance obtained with non-asbestos pixels was 35.958. This indicates no overlap in detection, with a difference between thresholds of 22.32, suggesting that the proposed method is suitable for detecting asbestos pixels in hyperspectral images. Once the asbestos detection threshold was identified, the proposed method was applied to the entire reference image (see Figure 7). For each pixel, the bands corresponding to the relevant peaks with a prominence greater than or equal to 0.02 and a height exceeding 0.196 were obtained. Subsequently, the Euclidean distance with the bands of the average pixel was calculated to determine whether this distance was less than 13.7. If the Euclidean distance between pixels was found to be less than 13.7, the pixel was marked in blue on a copy of the original image. Additionally, the detected asbestos pixels were counted, revealing that 11.872% of the pixels in the image correspond to asbestos.

```
arr_copia=np.copy(arr)
tam=arr_copia.shape
cont_pix=0
for i in range(tam[0]):
  for j in range(tam[1]):
    pix=arr_norm[i][j]
    cont=np.count_nonzero(pix)
    if(cont!=0):
      peaks, properties = find_peaks(pix[:300], prominence=0.02, height=0.196)
      if(len(peaks)<3):
        pic_pix=np.array([0,0,0])
      else:
        pic_pix=peaks[:3]

      dist=eu_norm(all_peaks, pic_pix)
      if(dist<13.7):
        arr_copia[i][j]=150
        cont_pix+=1
```

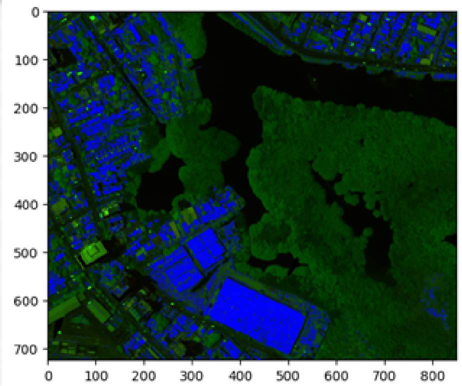

Figure 7. Application of the proposed method on the reference image.

To compare the effectiveness of the method, the correlation method was implemented on the entire reference image. For this, a correlation percentage was determined for each pixel in the image by comparing the characteristic or average pixel with each iterated pixel, using the previously calculated threshold of 99.27%, at which the correlation method shows no overlap.

```
[34] arr_copia=np.copy(arr)
     cont=0
     for i in range(arr.shape[0]):
       for j in range(arr.shape[1]):
         arr_temp=arr_norm[i][j]
         corr=ssd.correlation(pix_prom_asb, arr_temp)
         corr=corr/2
         porc=np.abs((1-corr)*100)
         if(porc>=99.27):
           arr_copia[i][j]=150
           cont+=1
```

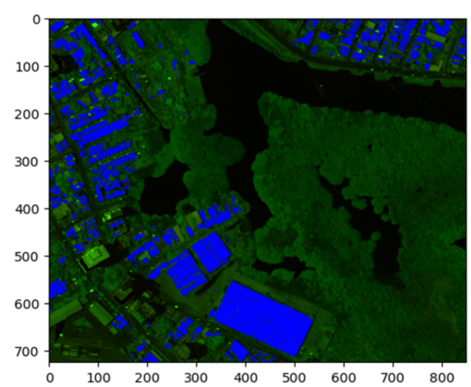

Figure 8. Application of the correlation method on the reference image.

Thus, when comparing the percentage of asbestos detected by each method, it was found that the relevant peaks method achieved an asbestos detection rate of 11.872% of pixels in the entire image, while the correlation method identified 9.85% (see Figure 9). This represents a detection difference of only 2.022% between the two methods, a variation that can be considered negligible given the large number of pixels comprising the analyzed image. This result suggests that the relevant peaks detection method is not only suitable for identifying asbestos in hyperspectral images but also demonstrates competitive performance compared to the correlation method, which is widely used in such analyses. Therefore, it can be inferred that the proposed method is a reliable alternative for asbestos detection applications, with a small margin of error relative to established methods.

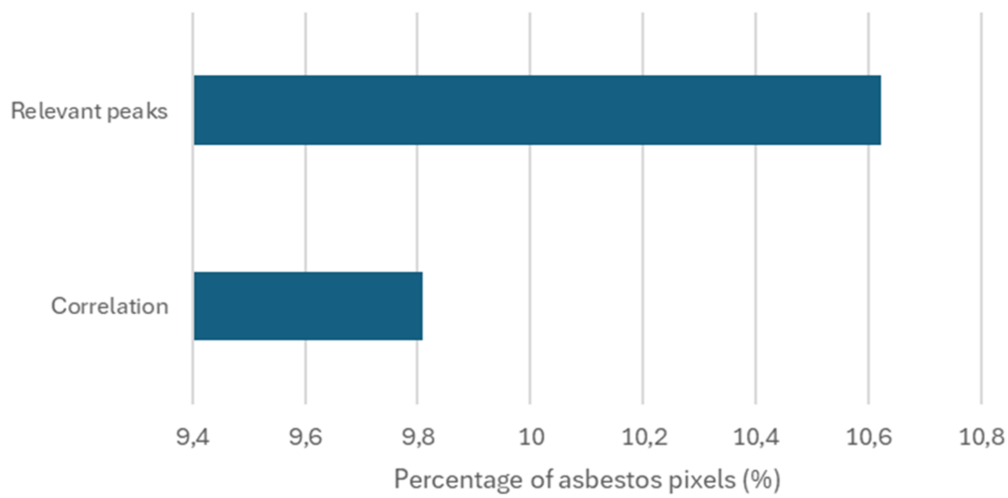

Figure 9. Percentage of asbestos detected using both methods.

To evaluate the efficiency of the proposed method compared to the correlation method, the average processing times for both methods were determined using Python's timeit library for a total of 20, 40, 60, 80, and 100 executions on a section of the reference hyperspectral image measuring 20x20 pixels and containing 380 bands. This was done to calculate the average time required by each method to process a region of the specified size and compare their efficiency. The comparative results obtained by recording the processing times for the proposed method and the correlation method across different numbers of executions are presented in Figure 10.

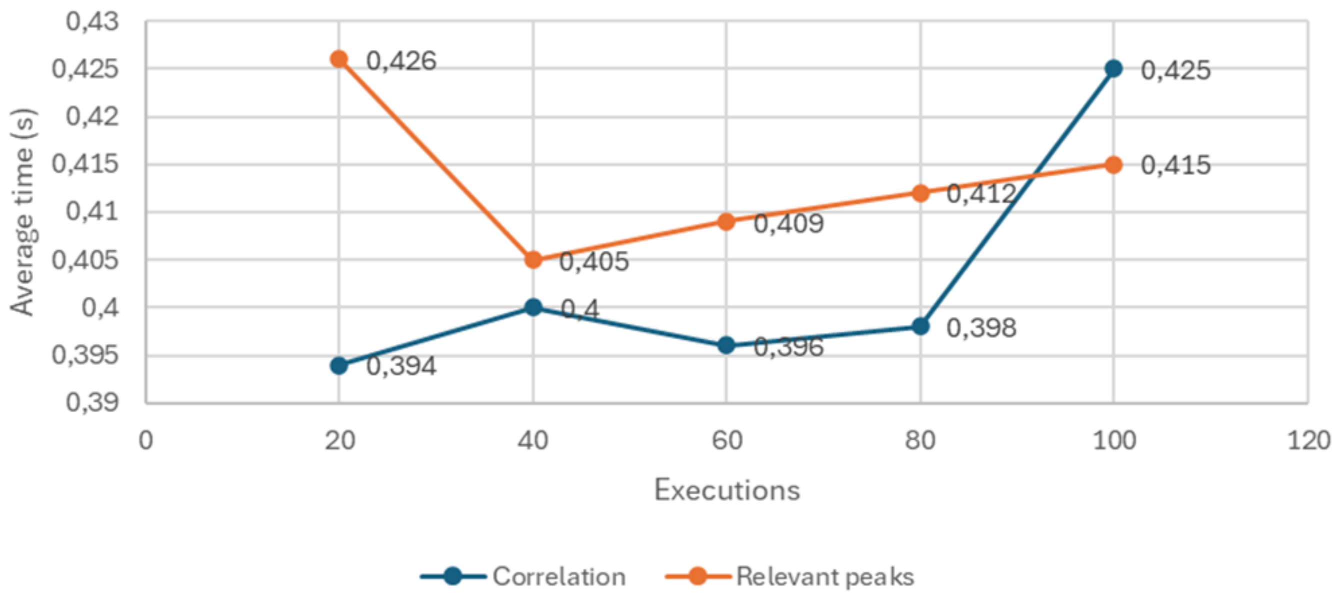

Figure 10. Average time by number of executions for both methods.

The analysis of processing times between the correlation method and the relevant peaks method indicates that both exhibit similar performance in terms of efficiency. On average, the correlation method records a processing time of 0.403 seconds, while the relevant peaks method reaches 0.413 seconds. Although there are initially more noticeable differences, such as in execution 20 where the relevant peaks method takes 0.426 seconds compared to 0.394 seconds for the correlation method, these differences decrease significantly as the number of executions increases, converging to similar values by execution 100 (0.425 s and 0.415 s, respectively). This demonstrates that, while the correlation method has a slight advantage on average, both methods are comparable in efficiency, particularly for higher numbers of executions. Therefore, the proposed method, in terms of both efficiency and effectiveness, can be considered for use in asbestos detection and integration into tools for detecting other materials, provided relevant peaks or those with higher prominence are identified and characterized beforehand.

At the discussion level of the results, it is important to highlight that this study proposed a new method for detecting asbestos-cement in hyperspectral images, which focuses on identifying the most relevant and prominent peaks of the characteristic spectral signature of asbestos-cement. This method demonstrated similar results in terms of effectiveness and efficiency compared to the correlation method, which is one of the most widely used approaches for material detection in hyperspectral images.

Accordingly, based on the obtained results, the proposed method constitutes a competitive alternative to material classification methods in hyperspectral images based on machine learning and deep learning, which, although effective, require significant computational resources due to the complexity of the models and the high dimensionality of the data (Islam et al., 2024; Zhang et al., 2020). In this regard, studies focused on asbestos detection using classification models, such as the one proposed in Bonifazi et al. (2024), could be replicated and adapted to the new method, aiming to enhance computational efficiency by leveraging the proposed approach, which offers similar effectiveness with lower computational complexity.

Finally, since the proposed method was implemented throughout the various phases of hyperspectral image processing and analysis using open-source libraries and technologies such as Spectral, NumPy, SciPy, and Matplotlib, this research represents an accessible alternative for research centers and universities in developing countries to facilitate experimentation with hyperspectral images. This makes it an excellent option for replicating and extrapolating studies conducted using proprietary software, such as the research by Valdelamar-Martínez et al. (2024), where the proprietary software ENVI was used.

4. Conclusions

One of the main challenges in hyperspectral image processing is developing efficient methods that can analyze the data cube and accurately detect materials without relying on computationally intensive approaches such as machine learning. The main objective of this research was to propose a novel non-machine-learning method for asbestos detection in hyperspectral images, based on identifying the most prominent peaks in the asbestos-cement spectral signature and selecting, through Euclidean distance, those that match the characteristic peaks of asbestos. By leveraging spectral peak differentiation, this approach provides an alternative to machine learning-based methods, offering a computationally efficient solution for asbestos detection. Additionally, the proposed method has the potential to be integrated into hyperspectral analysis tools for academic and industrial applications and can be adapted for the detection of other materials, provided their distinctive spectral peaks are characterized beforehand.

The method based on identifying the relevant peaks or maxima of the asbestos spectral curve has proven to be a viable and effective alternative for detecting this material in hyperspectral images. This is because the maximum Euclidean distance obtained for asbestos pixels (13.638) does not overlap with the minimum distance for non-asbestos pixels (35.958), confirming its ability to clearly differentiate between both types of pixels using the bands associated with the prominent peaks. Furthermore, when applying this method to the complete reference image, it successfully detected 11.872% of asbestos pixels, slightly exceeding the 9.85% detected by the correlation method. Since the percentage difference between the two methods is not significant, these results reinforce that the proposed approach is an effective and reliable option for asbestos identification in hyperspectral analysis.

When comparing the computational efficiency of the proposed method with the method based on the detection of relevant peaks, it was concluded that the proposed method presents a slight advantage on average, with a processing time of 0.403 seconds compared to 0.413 seconds for the relevant peaks method. However, the convergence of processing times at higher execution counts, such as at execution 100 (0.425 s and 0.415 s, respectively), demonstrates that both methods are comparable in terms of efficiency. This highlights the validity of the relevant peaks method as a viable alternative, offering competitive performance and consistent results, particularly in scenarios involving multiple executions.

This study demonstrated that open-source tools and libraries are an effective option for material detection in hyperspectral images, representing an accessible alternative to proprietary tools, whose high costs limit their use within the academic community. In particular, the Spectral library proved highly useful for extracting the spectral band data from the image used in this research. Similarly, the SciPy library was fundamental for detecting the most prominent peaks in the asbestos curve using the fi d_peaks() method. Additionally, the NumPy library was instrumental in calculating the Euclidean distance between the bands of the relevant peaks in the asbestos curve and the bands of the relevant peaks in other pixels. Likewise, the Pandas library was useful for loading the data points corresponding to the asbestos and non-asbestos sample pixels. Finally, the Matplotlib library facilitated the generation of graphs for the asbestos pixels, non-asbestos pixels, and the characteristic pixel.

The efficiency of the asbestos pixel detection method is improved by reducing the dimensionality of the hyperspectral image, discarding less relevant bands within the range of 0 to 300, as bands 300 to 380 were already excluded in this study. Additionally, the method's effectiveness is enhanced by incorporating the analysis of relevant minima in the curve, creating a band array composed of both the minima and maxima of the spectral curve.

4. Acknowledgements

The University of Cartagena, Colombia, and the Asbestos-Free Colombia Foundation executed this project.

Authors' contribution

Gabriel Elías Chanchí-Golondrino: Conceptualization, Data curation, Software, Writing -original draft.

Manuel Alejandro Ospina-Alarcón: Formal analysis, Investigation, Methodology, Validation and Writing -review editing.

Manuel Saba: Funding acquisition, Project administration, Resources, Supervision, Writing -review editing

Ethical implications

There are no ethical implications to state in writing or publishing this article.

Funding

This article is considered a product in the framework of the project: "Formulation of an integral strategy to reduce the impact on public and environmental health due to the presence of asbestos in the territory of the Department of Bolivar," financed by the General System of Royalties of Colombia (SGR) and identified with the code BPIN 2020000100366.

Conflicts of interest

There are no conflicts of interest from the authors in the writing or publication of this article.

5. References

Abbasi, M., Mostafa, S., Vieira, A. S., Patorniti, N., & Stewart, R. A. (2022). Mapping Roofing with Asbestos-Containing Material by Using Remote Sensing Imagery and Machine Learning-Based Image Classification: A State-of-the-Art Review. Sustainability, 14 (13), 8068. https://doi.org/10.3390/su14138068

Adão, T., Hruška, J., Pádua, L., Bessa, J., Peres, E., Morais, R., & Sousa, J. (2017). Hyperspectral Imaging: A Review on UAV-Based Sensors, Data Processing and Applications for Agriculture and Forestry. Remote Sensing, 9 (11), 1110. https://doi.org/10.3390/rs9111110

Ai, W., Liu, S., Liao, H., Du, J., Cai, Y., Liao, C., Shi, H., Lin, Y., Junaid, M., Yue, X., & Wang, J. (2022). Application of hyperspectral imaging technology in the rapid identification of microplastics in farmland soil. Science of the Total Environment, 807, 151030. https://doi.org/10.1016/j.scitotenv.2021.151030

Ang, K. L.-M., & Seng, J. K. P. (2021). Big Data and Machine Learning With Hyperspectral Information in Agriculture. IEEE Access, 9, 36699–36718. https://doi.org/10.1109/ACCESS.2021.3051196

Bodkin, A., Sheinis, A., Norton, A., Daly, J., Beaven, S., & Weinheimer, J. (2009). Snapshot hyperspectral imaging: the hyperpixel array camera. In S. S. Shen & P. E. Lewis (Eds.), Algorithms and Technologies for Multispectral, Hyperspectral, and Ultraspectral Imagery XV, 73340H. https://doi.org/10.1117/12.818929

Bonifazi, G., Capobianco, G., & Serranti, S. (2015). Hyperspectral imaging applied to the identification and classification of asbestos fibers. 2015 IEEE SENSORS, 1–4. https://doi.org/10.1109/ICSENS.2015.7370458

Bonifazi, G., Capobianco, G., & Serranti, S. (2018). Asbestos containing materials detection and classification by the use of hyperspectral imaging. Journal of Hazardous Materials, 344, 981–993. https://doi.org/10.1016/j.jhazmat.2017.11.056

Bonifazi, G., Capobianco, G., & Serranti, S. (2019). Hyperspectral Imaging and Hierarchical PLS-DA Applied to Asbestos Recognition in Construction and Demolition Waste. Applied Sciences, 9 (21), 4587. https://doi.org/10.3390/app9214587

Bonifazi, G., Capobianco, G., Serranti, S., Trotta, O., Bellagamba, S., Malinconico, S., & Paglietti, F. (2024). Asbestos detection in construction and demolition waste by different classification methods applied to short-wave infrared hyperspectral images. Spectrochimica Acta Part A: Molecular and Biomolecular Spectroscopy, 307, 123672. https://doi.org/10.1016/j.saa.2023.123672

Calvillo, E. A., Mendoza, R., Munoz, J., Martinez, J. C., Vargas, M., & Rodriguez, L. C. (2016). Automatic algorithm to classify and locate research papers using natural language. IEEE Latin America Transactions, 14 (3), 1367–1371. https://doi.org/10.1109/TLA.2016.7459622

Ding, X., Zhang, S., & Li, H. (2016). A Polymorphic Ant Colony Algorithm (PACA) for the Selection of Optimized Band Selection of Hyperspectral Remote Sensing Image. Proceedings of the 2016 International Conference on Engineering and Technology Innovations. https://doi.org/10.2991/iceti-16.2016.37

Eckhard, J., Eckhard, T., Valero, E. M., Nieves, J. L., & Contreras, E. G. (2015). Outdoor scene reflectance measurements using a Bragg-grating-based hyperspectral imager. Applied Optics, 54 (13), D15. https://doi.org/10.1364/AO.54.000D15

Eismann, M. T. (2012). Hyperspectral Remote Sensing. SPIE. https://doi.org/10.1117/3.899758

Espinosa-Zúñiga, J. J. (2020). Aplicación de metodología CRISP-DM para segmentación geográfica de una base de datos pública. Ingeniería, Investigación y Tecnología, 21 (1), 1–13. https://doi.org/10.22201/fi.25940732e.2020.21n1.008

Frassy, F., Candiani, G., Rusmini, M., Maianti, P., Marchesi, A., Nodari, F., Via, G., Albonico, C., & Gianinetto, M. (2014). Mapping Asbestos-Cement Roofing with Hyperspectral Remote Sensing over a Large Mountain Region of the Italian Western Alps. Sensors, 14 (9), 15900–15913. https://doi.org/10.3390/s140915900

Gao, L., & Smith, R. T. (2015). Optical hyperspectral imaging in microscopy and spectroscopy - a review of data acquisition. Journal of Biophotonics, 8 (6), 441–456. https://doi.org/10.1002/jbio.201400051

Gao, L., Yao, D., Li, Q., Zhuang, L., Zhang, B., & Bioucas-Dias, J. (2017). A New Low-Rank Representation Based Hyperspectral Image Denoising Method for Mineral Mapping. Remote Sensing, 9 (11), 1145. https://doi.org/10.3390/rs9111145

González-Núñez, H., & de la Fuente, R. (2017). Offner imaging spectrometers. Optica Pura y Aplicada, 50 (1), 37–47. https://doi.org/10.7149/OPA.50.1.49506

González, C., Resano, J., Mozos, D., Plaza, A., & Valencia, D. (2010). FPGA Implementation of the Pixel Purity Index Algorithm for Remotely Sensed Hyperspectral Image Analysis. EURASIP Journal on Advances in Signal Processing, 2010 (1), 969806. https://doi.org/10.1155/2010/969806

Gu, Y., Liu, T., Gao, G., Ren, G., Ma, Y., Chanussot, J., & Jia, X. (2021). Multimodal hyperspectral remote sensing: an overview and perspective. Science China Information Sciences, 64 (2), 121301. https://doi.org/10.1007/s11432-020-3084-1

Islam, T., Islam, R., Uddin, P., & Ulhaq, A. (2024). Spectrally Segmented-Enhanced Neural Network for Precise Land Cover Object Classification in Hyperspectral Imagery. Remote Sensing, 16 (5), 807. https://doi.org/10.3390/rs16050807

Kaplan, G., Gašparović, M., Kaplan, O., Adjiski, V., Comert, R., & Mobariz, M. A. (2023). Machine Learning-Based Classification of Asbestos-Containing Roofs Using Airborne RGB and Thermal

Imagery. Sustainability, 15 (7), 6067. https://doi.org/10.3390/su15076067

Kapre, A., Kunde, S., Mittal, S., & Singhal, R. (2023). RAxC: Reflexivity-based Approximate Computing techniques for efficient remote sensing. 2023 IEEE International Conference on Big Data (BigData), 1168–1173. https://doi.org/10.1109/BigData59044.2023.10386511

Khan, M. J., Khan, H. S., Yousaf, A., Khurshid, K., & Abbas, A. (2018). Modern Trends in Hyperspectral Image Analysis: A Review. IEEE Access, 6, 14118–14129. https://doi.org/10.1109/ACCESS.2018.2812999

Lim, H.-T., & Murukeshan, V. M. (2017). Spatial calibration and image processing requirements of an image fi er bundle based snapshot hyperspectral imaging probe: from raw data to datacube. In A. K. Asundi (Ed.), Fifth International Conference on Optical and Photonics Engineering, 104491P. https://doi.org/10.1117/12.2270739

Lu, B., Dao, P., Liu, J., He, Y., & Shang, J. (2020). Recent Advances of Hyperspectral Imaging Technology and Applications in Agriculture. Remote Sensing, 12 (16), 2659. https://doi.org/10.3390/rs12162659

Martinez-Plumed, F., Contreras-Ochando, L., Ferri, C., Hernandez-Orallo, J., Kull, M., Lachiche, N., Ramirez-Quintana, M. J., & Flach, P. (2021). CRISP-DM Twenty Years Later: From Data Mining Processes to Data Science Trajectories. IEEE Transactions on Knowledge and Data Engineering, 33 (8), 3048–3061. https://doi.org/10.1109/TKDE.2019.2962680

Mendes, V. B., Leta, F. R., Conci, A., & Gonçalves, L. B. (2010). Detección de Posición Angular de Embarcaciones, utilizando Técnicas de Visión Computacional y Redes Neurales Artificiales. Información Tecnológica, 21 (6). https://doi.org/10.4067/S0718-07642010000600018

Moroni, M., Lupo, E., Marra, E., & Cenedese, A. (2013). Hyperspectral Image Analysis in Environmental Monitoring: Setup of a New Tunable Filter Platform. Procedia Environmental Sciences, 19, 885–894. https://doi.org/10.1016/j.proenv.2013.06.098

Padhan, P. C., & others. (2012). Application of ARIMA model for forecasting agricultural productivity in India. Journal of Agriculture and Social Sciences, 8 (2), 50–56.

Paoletti, M. E., Haut, J. M., Plaza, J., & Plaza, A. (2019). Estudio Comparativo de Técnicas de Clasificación de Imágenes Hiperespectrales. Revista Iberoamericana de Automática e Informática Industrial, 16 (2), 129. https://doi.org/10.4995/riai.2019.11078

Park, B. (2016). Future Trends in Hyperspectral Imaging. NIR News, 27 (1), 35–38. https://doi.org/10.1255/nirn.1583

Pérez-Roncal, C., López-Maestresalas, A., López-Molina, C., Marín-Ederra, D., Urrestarazu-Vidart, J., Arazuri-Garín, S., Santesteban-García, L. G., & Jarén-Ceballos, C. (2019). Identificación de la presencia de oídio (Erysiphe necator) en racimos de uva mediante imágenes hiperespectrales. Congreso Ibérico de Agroingeniería, 1248–1254. https://doi.org/10.26754/c_agroing.2019.com.3434

Peyghambari, S., & Zhang, Y. (2021). Hyperspectral remote sensing in lithological mapping, mineral exploration, and environmental geology: an updated review. Journal of Applied Remote Sensing, 15 (03). https://doi.org/10.1117/1.JRS.15.031501

Sahoo, R. (2020). Hyperspectral Remote Sensing. Elsevier. https://doi.org/10.1016/C2018-0-01850-2

Tan, K., Wang, H., Chen, L., Du, Q., Du, P., & Pan, C. (2020). Estimation of the spatial distribution of heavy metal in agricultural soils using airborne hyperspectral imaging and random forest. Journal of Hazardous Materials, 382, 120987. https://doi.org/10.1016/j.jhazmat.2019.120987

Valdelamar-Martínez, D., Saba, M., & Torres-Gil, L. K. (2024). Assessment of asbestos-cement roof distribution and prioritized intervention approaches through hyperspectral imaging. Heliyon, 10 (3), e25612. https://doi.org/10.1016/j.heliyon.2024.e25612

Wang, C., Liu, B., Liu, L., Zhu, Y., Hou, J., Liu, P., & Li, X. (2021). A review of deep learning used in the hyperspectral image analysis for agriculture. Artificial Intelligence Review, 54 (7), 5205–5253. https://doi.org/10.1007/s10462-021-10018-y

Yi, L., Chen, J. M., Zhang, G., Xu, X., Ming, X., & Guo, W. (2021). Seamless Mosaicking of UAV-Based Push-Broom Hyperspectral Images for Environment Monitoring. Remote Sensing, 13 (22), 4720. https://doi.org/10.3390/rs13224720

Zhang, L., & Zhong, Y. (2010). Analysis of Hyperspectral Remote Sensing Images. In Geospatial Technology for Earth Observation, 235–269. Springer US. https://doi.org/10.1007/978-1-4419-0050-0_9

Zhang, X., Wang, Y., Zhang, N., Xu, D., Luo, H., Chen, B., & Ben, G. (2020). SSDANet: Spectral-Spatial Three-Dimensional Convolutional Neural Network for Hyperspectral Image Classification. IEEE Access, 8, 127167–127180. https://doi.org/10.1109/ACCESS.2020.3008029fgjgh